Electrical properties of yttrium iron garnet

Electrical Properties of Yttrium Iron Garnet (*).

R. METSELAAR

Department of Physical Chemistry, Eindhoven University of Technology Eindhoven, The Netherlands

P. K. LARSEN

Philips Research Laboratories - Eindhoven, The Netherlands

1. – Introduction.

The study of the electrical transport properties of yttrium iron garnet (YIG, $Y_3Fe_5O_{12}$) was started in 1957 by VAN UITERT and SWANEKAMP [1]. Since then a great number of investigations of the electrical properties of YIG have taken place—some in combination with studies of other properties like the magnetic and optical properties [2-18]. Measurements of the photoconductivity of YIG have also been performed [19-21]. The results and conclusions of many of these studies often seem contradictory, *e.g.* different conductivities are given for similar doped samples and both band conduction and hopping conduction have been proposed. The apparent discrepancies can be ascribed to various causes. The preparation of well-defined samples is not easy, the conductivity is relatively small due to small mobilities of the charge carriers, so that (Hall) measurements are difficult, and the ionic nature of YIG leads to different points of view concerning the interpretation of experimental results.

Yttrium iron garnet is a transition metal compound and the presence of the iron $3d$ ions does not only give rise to the magnetic properties or the high optical absorption in the visible and near infra-red wavelength range, it also has a profound influence on the electrical properties. A garnet like $Gd_3Ga_5O_{12}$ is a good insulator ($\varrho > 10^{15}\ \Omega$ cm at 300 K) and cannot be made semiconducting. YIG which may be insulating ($\varrho \geqslant 10^{12}\ \Omega$ cm at 300 K) can easily be doped with tetravalent or divalent impurities, so that it becomes semiconducting ($\varrho \sim 10^{4}\ \Omega$ cm at 300 K). Due to the little overlap in solids of $3d$ states with the states on neighbouring ions one expects that relatively narrow d-bands

(*) Seminar held by R. METSELAAR.

are formed. In YIG, iron ions are found on octahedral and tetrahedral coordinated sites, and, if we take into account the crystal field splitting, the d-bands are composed of (four) subbands. Optical measurements show that this is the case for the empty conduction band derived from Fe^{2+} states [22-25]. The subbands may partly overlap in energy, so that a broadened d-band is formed. Photoemission measurements indicate this for the valence band derived from Fe^{3+} states, which partly overlaps with the broad oxygen $2p$ band [26].

It is widely assumed that Fe^{2+} and Fe^{4+} ions are formed if tetravalent respectively divalent impurities are added to YIG and that the Fe^{2+} or Fe^{4+} concentration equals the corresponding impurity concentration [27]. In this localized picture, electrical conduction takes place via a hopping mechanism with a temperature-independent number of charge carriers and a mobility characterized by an activation energy. In contrast, the number of charge carriers in the band model is determined by an ionization energy and varies exponentially with temperature, while the mobility is rather temperature independent. In the analysis of experimental data it is important not to exclude any of the models *a priori*. In the theory presented in sect. **2** the localized model discussed above can be considered as a (special) case of small-polaron hopping conduction.

The fact that YIG should be considered as a partially compensated semiconductor has often been neglected. Many experiments were performed on silicon-doped YIG single crystals, which have to be grown from a flux, generally a mixture of PbO and B_2O_3. Since the distribution coefficient of the silicon dopant, between melt and crystal, is not equal to one and varies with growth conditions, the nominal silicon concentrations cited in earlier literature cannot be trusted. Even if a chemical analysis is carried out, the problem of a possible inhomogeneous distribution of the impurities remains. A consequence of the flux growth process is also that lead ions are always present as a counter-dope in the crystals. From chemical analysis a Fe^{2+} or Fe^{4+} concentration is often given. It should here be remembered that actually the reducing or oxidizing power is measured, which is determined by the difference of the concentrations of majority and minority centres.

When polycrystalline samples are used, the standard ceramic preparation technique of ball milling generally produces samples with a high impurity content. Improper cooling of the sintered product can easily lead to the formation of high-ohmic grain boundaries. In general the cooling procedure after a heat treatment of the iron garnet can strongly influence the physical properties via the number of oxygen vacancies.

In sect. **2** the appropriate theoretical equations for the analysis of experimental data are given. In sect. **3** and **4**, respectively, we shall review the experimental data for temperatures below about $(400 \div 500)$ K and at temperatures in the range $(500 \div 1500)$ K. Special attention will be paid to the nature of the charge carriers.

2. – Theory.

In this section the theoretical background needed for the analysis of the electrical measurements performed on YIG will be presented. A more extensive description has been given by BOSMAN and VAN DAAL [28]. For a general discussion of semiconductor statistics and, in particular, partially compensated semiconductors we refer the reader to BLAKEMORE [29].

2·1. *D.c. conductivity, Seebeck effect and Hall effect.* – The d.c. conductivity σ is the sum of the contributions of positive and negative charge carriers

$$\sigma = \sigma_+ + \sigma_- = pe\mu_+ + ne\mu_- . \tag{1}$$

Here, e is the absolute value of the electronic charge, p and n are the concentration of positive and negative charge carriers, and μ_+ and μ_- are the respective mobilities. The concentrations n and p can be written in terms of the effective densities of states N_+ and N_- for the valence and the conduction band, respectively, the Fermi energy E_F and the energies E_v and E_c of, respectively, the top of the uppermost valence band and the bottom of the lowest conduction band:

$$p = N_+ \exp[(E_v - E_F)/kT] , \tag{2a}$$

$$n = N_- \exp[(E_F - E_c)/kT] . \tag{2b}$$

If we write $E_g = E_c - E_v$ for the band gap energy, we get

$$np = N_+ N_- \exp[-E_g/kT] . \tag{3}$$

From eqs. (1) and (3) it follows that σ reaches a minimum value

$$\sigma_{min} = 2e(\mu_+ \mu_- N_+ N_-)^{\frac{1}{2}} \exp[-E_g/2kT] , \tag{4}$$

when $\sigma_+ = \sigma_- = \frac{1}{2}\sigma_{min}$.

The Seebeck coefficient α can be expressed in the partial Seebeck coefficients α_+ and α_- by

$$\alpha = (\sigma_+ \alpha_+ + \sigma_- \alpha_-)/(\sigma_+ + \sigma_-) , \tag{5}$$

where

$$\alpha_+ = (k/e)[\ln (N_+/p) + A_+] , \tag{6a}$$

$$\alpha_- = -(k/e)[\ln (N_-/n) + A_-] . \tag{6b}$$

Here A_+ and A_- are the transport constants. For $\sigma = \sigma_{\min}$ the Seebeck coefficient has the value

$$\alpha_i = (k/2e) \ln (N_+ e^{A_+} \mu_+ / N_- e^{A_-} \mu_-) . \tag{7}$$

The Hall coefficient R_0 can be obtained from the partial Hall coefficients R_+ and R_- via

$$R_0 = (R_+ \sigma_+^2 + R_- \sigma_-^2)/(\sigma_+ + \sigma_-)^2 \tag{8}$$

with

$$R_+ = 1/pe , \tag{9a}$$

$$R_- = -1/ne . \tag{9b}$$

For a magnetic conductor there is an anomalous Hall effect superposed on the ordinary Hall effect in the temperature region below the Curie point. The Hall resistivity ϱ_H, which is the Hall voltage normalized with respect to sample geometry and current, can be written as

$$\varrho_H = R_0 B + R_e M , \tag{10}$$

where R_e is the anomalous Hall coefficient, B the internal magnetic field and M the magnetization.

In some magnetic semiconductors like the ferromagnetic sulpho-spinels the electrical properties are strongly influenced by the magnetic properties. Such an interaction can be caused by various mechanisms, *e.g.* exchange splitting of the bands, spin-disorder scattering influencing the mobility or magnetic impurity state conduction. For YIG the electrical properties are only influenced very little by the magnetization and no special consideration to this point is needed.

2·2. *Large and small polarons.* – It was shortly mentioned in the introduction and will be seen in sect. **3** that the mobilities of charge carriers in YIG are small. The charge carriers should therefore be regarded as polarons. This is not surprising, since YIG is an ionic compound. We shall here shortly discuss the large and the small polaron.

If the lattice distortion, induced by the charge carrier, extends over distances larger than the lattice distance, we have to use the large-polaron band model. It can be shown that there is a lower limit of the value of the drift mobility for consistency with the band scheme. A value of $\mu \geqslant 1$ cm^2/Vs is representative. The effective density of states in this case is given by

$$N_\pm = 2(2\pi m_\pm^* kT/h^2)^{\frac{3}{2}} , \tag{11}$$

where $m_{\pm}^{*}$ is the effective mass of the polaron. At temperatures below the Debye temperature θ_D, $T \ll \theta_D$, the drift mobility of a large polaron is dominated by a term $\exp[\theta_D/T]$ when optical lattice modes are the main scatterers. In the case that ionized impurities serve as scattering sites, the drift mobility varies as $T^{\frac{3}{2}}$. At high temperatures the temperature dependence of the mobility is mainly determined by scattering of charge carriers with lattice vibrations, which gives $\mu \propto T^{-\frac{3}{2}}$. For the band model the product of the effective density of states times the drift mobility should therefore be nearly temperature independent at high temperatures. We finally want to remark that the transport constants $A_{\pm}$ which occur in the expressions for the Seebeck coefficients are about 2 in the large-polaron model.

If the interaction between the charge carrier and the lattice is strong and the band is narrow, the charge carrier can be trapped in its own self-generated polarization field in the ionic lattice. This is the case of the small polaron, where the charge carrier becomes localized within the size of a lattice distance. At low temperatures, $T < 0.4\ \theta_D$, small-polaron band conduction might be possible. However, we shall here only consider the phonon-assisted small-polaron hopping conduction. An upper limit of the mobility in the hopping region is estimated to be $\mu \ll 0.1\ \mathrm{cm^2/Vs}$. The density of states is in this case twice the concentration of cations available as a site for the small polaron. For YIG, for instance, small-polaron hopping via the octahedral sites would mean $N = 8.4 \cdot 10^{21}\ \mathrm{cm^{-3}}$ [17], whereas eq. (11) at 300 K gives $N = 2.5 \cdot 10^{19} \cdot (m^*/m)^{\frac{3}{2}}\ \mathrm{cm^{-3}}$. The temperature dependence of the drift mobility is of the form

$$\mu = \mu_0 T^{-\frac{3}{2}} \exp[-U/kT], \tag{12}$$

where U is the hopping energy. It should here be remembered that for the temperature dependence of the conductivity also the ionization energy of the charge carriers from the appropriate donor or acceptor centres is a determining factor. The transport constant for the small polaron is very small, $A \sim 0$.

We finally want to mention that also a paramagnetic polaron has been proposed [30]. In this model the spins around the charge carrier are polarized to form the magnetic polaron. As mentioned above, the electrical properties in YIG are only very little dependent on the magnetization and we shall therefore not discuss this model further.

2·3. *Dielectric-relaxation losses.* – If electrical dipoles exist in the solid, *e.g.* formed by the localization of a charge carrier at one of the neighbouring cations of the centre delivering the charge carrier, dielectric relaxation can take place. Under the influence of an applied electric field a partial alignment of the dipoles takes place, with a characteristic relaxation time τ. The cor-

responding complex dielectric constant $\varepsilon_1 + i\varepsilon_2$ has the form

$$\varepsilon_1 = \varepsilon_\infty + (\varepsilon_s - \varepsilon_\infty)/(1 + \omega^2\tau^2), \tag{13a}$$

$$\varepsilon_2 = (\varepsilon_s - \varepsilon_\infty)\omega\tau/(1 + \omega^2\tau^2), \tag{13b}$$

$$\operatorname{tg}\delta = \varepsilon_2/\varepsilon_1 = (\varepsilon_s - \varepsilon_\infty)\omega\tau/(\varepsilon_s + \varepsilon_\infty\omega^2\tau^2), \tag{13c}$$

where ε_s is the static value of the dielectric constant, ε_∞ is the value at frequencies for which $\omega\tau \gg 1$, and $\operatorname{tg}\delta$ is the dielectric-relaxation loss function. The real part of the a.c. conductivity, $\sigma(\omega)$, is related to ε_2 by

$$\sigma(\omega) = \omega\varepsilon_2/4\pi. \tag{14}$$

From a measurement of $\varepsilon_s - \varepsilon_\infty$ the dipole moment can be evaluated:

$$\varepsilon_s - \varepsilon_\infty = 4\pi N p^2/bkT. \tag{15}$$

Here N is the concentration of dipoles, p the dipole moment and b a constant having a value of approximately 2.5.

2·4. *Extrinsic and intrinsic conductivity range.* – It is useful to distinguish between the extrinsic conductivity range, where σ and α are determined by one type of carriers only, *e.g.* $\sigma \sim \sigma_-$ and $\alpha \sim \alpha_-$, and the intrinsic conductivity range, where σ_+ and σ_- are of the same magnitude. The latter range is normally of importance at elevated temperatures.

In the extrinsic p-type conduction region eq. (1) gives for the resistivity $\varrho = 1/\sigma$:

$$\log\varrho = -\log(pe\mu_+). \tag{16}$$

By introducing a reduced Seebeck coefficient $\alpha'_+ = \alpha_+ e/k \ln 10$, it follows from eq. (6*a*) that

$$\alpha'_+ = A_+/\ln 10 + \log(N_+/p). \tag{17}$$

For the case of band conduction (large-polaron conduction) the product $N_+\mu_+$ does not vary with temperature and eq. (17) can be written as

$$\alpha'_+ = \text{const} - \log(p\mu_+). \tag{18}$$

Comparison of eqs. (16) and (18) shows that in this case plots of $\log\varrho$ and of α'_+ *vs.* T^{-1} give straight lines with equal slopes.

For the case of small-polaron conduction $N_+ = \text{const}$, so that eq. (17)

reduces to

$$\alpha'_+ = \text{const} - \log p \,. \tag{19}$$

Substitution of eq. (12) in eq. (16) shows that the slope of $\log \varrho$ *vs.* T^{-1} exceeds the slope of α' *vs.* T^{-1} and the difference in the slopes is just equal to U/k (the influence of the $T^{-\frac{3}{2}}$ term in eq. (12) can be neglected for a restricted temperature range). In practice, however, it is difficult to distinguish between the two conduction mechanisms in this way, since the expected value of U is only of the order of 0.1 eV, that is of the order of kT.

In the case that the hole concentration $p \ll N_a - N_d$, $N_a > N_d$, where N_a and N_d are the acceptor respectively the donor concentrations, the temperature dependence of the Fermi energy can be approximated with

$$E_F - E_v = E_a - kT \ln[(N_a - N_d)/g_+ N_d] \,, \tag{20}$$

where E_a is the ionization energy of the acceptors and g_+ is the degeneracy factor of the acceptor centre. Combination of eqs. (2), (6), (20) shows that

$$\alpha'_+ \ln 10 = E_a/kT + \ln(g_+ e^{A_+}) - \ln[(N_a - N_d)/N_d] \,. \tag{21}$$

Equations analogous to eqs. (16)-(21) are obtained for an extrinsic n-type conductor. Thus, from the slope of the α' *vs.* T^{-1} plot, we can obtain E_a if $p \ll N_a - N_d$. When the degree of compensation is known, the intercept of the curve at $T^{-1} = 0$ can be used to determine the product ge^A. These equations hold irrespective of the conduction mechanism.

In the intrinsic conductivity range we have to use eqs. (1) and (5). A useful approach to the two-carrier analysis has been given by JONKER [31]. He combined the expressions for σ and α into

$$\alpha e/k = \pm \frac{1}{2}\varepsilon[1 - (\sigma_{\min}/\sigma)^2]^{\frac{1}{2}} - \ln\left(\frac{\sigma}{\sigma_{\min}}\left\{1 \pm \left[1 - \left(\frac{\sigma_{\min}}{\sigma}\right)^2\right]^{\frac{1}{2}}\right\}\right) + \alpha_i \,, \tag{22}$$

where the + and − signs are valid for $\sigma_+ \geqslant \frac{1}{2}\sigma_{\min}$ and $\sigma_- \geqslant \frac{1}{2}\sigma_{\min}$, respectively. α_i is the value of the Seebeck coefficient at $\sigma = \sigma_{\min}$ as given in eq. (7). The parameter ε is

$$\varepsilon = E_g/kT + A_+ + A_- \,. \tag{23}$$

When α is plotted as a function of $\ln(\sigma/\sigma_{\min})$, the resulting curve has the shape of a pear and is referred to as «Jonker's pear». It is important to note that eq. (22) also is valid in the extrinsic conductivity range and that the α *vs.* $\ln(\sigma/\sigma_{\min})$ plot in the case of band conduction depends only on the intrinsic parameter ε. This means that the correctness of simultaneous measurements of α and σ can be checked by their fit to the appropriate Jonker's pear. This

fit is independent of doping, so that it can be used to compare data obtained on different samples. From eqs. (1) and (6) it follows that for the extrinsic p-type region (compare eq. (18))

$$\alpha_+ e/k = \ln (N_+ e^{A_+} \mu_+ e) - \ln \sigma . \tag{24}$$

In Jonker's pear this leads to a straight line with slope -1 for the p-type region, and analogously to a straight line with slope $+1$ for the extrinsic n-type region. Thus, independent of doping and temperature, all data obtained in the extrinsic range should fit the same straight lines, if indeed $N_+\mu_+$ and $N_-\mu_-$ are constant, independent of the temperature. In the case of small-polaron hopping conduction a temperature-dependent parallel shift of the straight lines should be seen.

2·5. *Impurity and inhomogeneous conduction.* – In partially compensated solids where the majority centres (*e.g.* donor centres) are partly unoccupied due to the presence of minority centres (acceptor centres), the charge carriers (electrons) may jump from an occupied to a neighbouring unoccupied majority centre. The hopping process is photon induced and shows a thermally activated character. The total conductivity σ_{tot} consists of the normal contribution σ and the impurity contribution σ_{imp}: $\sigma_{tot} = \sigma + \sigma_{imp}$. The thermal activation energy determining σ_{imp} is smaller than the ionization energy of the majority centres, so that σ_{imp} only dominates at low temperatures.

In polycrystalline samples the impurity centres may not be uniformly distributed over grains and grain boundaries and the electrical properties can become significantly affected if this results in a conductivity of the grain boundaries different from that of the grains. A description of a macroscopic inhomogeneous solid in terms of a two-layer model has been given by KOOPS [32]. Let the grain boundaries and grains have thicknesses d_1 and d_2 and d.c. conductivities σ_1 and σ_2, respectively. We assume that the relative dielectric permittivity ε_i is equal for the two layers and independent of the frequency. We have $d_1 \ll d_2$ and if, furthermore, $\sigma_1/d_1 \ll \sigma_2/d_2$ (high-ohmic grain boundaries), one finds

$$\varepsilon_1(\omega) = (\varepsilon_s + \varepsilon_\infty \omega^2\tau^2)/(1 + \omega^2\tau^2) , \tag{25a}$$

$$\sigma(\omega) = (\sigma_s + \sigma_\infty \omega^2\tau^2)/(1 + \omega^2\tau^2) , \tag{25b}$$

where

$$\varepsilon_s \approx \varepsilon_i(d_1 + d_2)/d_1 , \qquad \varepsilon_\infty = \varepsilon_i , \tag{26a}$$

$$\sigma_s \approx \sigma_1(d_1 + d_2)/d_1 , \qquad \sigma_\infty \approx \sigma_2 d_2/(d_1 + d_2) \tag{26b}$$

and

$$\tau \approx \varepsilon_0(\varepsilon_s - \varepsilon_\infty)/(\sigma_\infty - \sigma_s) . \tag{26c}$$

Equation (26*a*) shows that very high static dielectric permittivities may be found. It is further seen that the temperature dependence of the relaxation time τ is characterized by the temperature dependence of σ_2, because $\sigma_s \ll \sigma_\infty$.

The static conductivity σ_s may depend on the applied voltage, *i.e.* show a nonohmic behaviour. In a barrier model introduced by HEYWANG it is assumed that the majority impurity centres are uniformly distributed over the grains and the grain boundaries [33]. In the boundary layers, minority centres, which may be boundary surface states, are accumulated and a potential barrier is formed. The space charge zone will be displaced under an applied potential and the potential barrier will be lowered. The current through a slab of thickness L is given by

$$i \propto f(V/L)\,, \tag{27}$$

so that deviations from Ohm's law should show the same dependence on the applied voltage V and $1/L$.

In another barrier model proposed by LARSEN and METSELAAR deviations from Ohm's law are explained as a consequence of space charge injection into the grain boundaries [12, 13]. When the conductance of these is small compared to that of the grains, the voltage drop over the grains is much smaller than the voltage drop over the grain boundaries. Due to the small value of d_1, the electric field and thus the space charge in the boundaries can be very high. In accordance with the theory of space-charge limited currents in homogeneous solids, the current in this region can be written [34] as

$$i \propto V^\gamma / L^\beta\,, \tag{28}$$

where γ and β are temperature-dependent constants, $\gamma \geqslant 2$ and $\beta - 1 = 2(\gamma - 1)$.

3. – Low-temperature results.

In this section we shall consider the experimental results at temperatures below about 600 K.

3·1. *D.c. measurements.* – The first extensive electrical measurements on doped YIG were performed by VERWEEL and ROOVERS [2]. They measured the d.c. conductivity and the Seebeck coefficient of series of polycrystalline samples $Y_{3-y}Ca_yFe_5O_{12}$ and $Y_3Fe_{5-x}Si_xO_{12}$. The Ca-doped samples with $y > 0.01$ were p-type having a conductivity up to $10^{-2}\,(\Omega\ \mathrm{cm})^{-1}$ at 40° C with an activation energy of 0.3 eV. Recently JONKER [35] prepared Ca-doped single crystals of YIG. Our measurements on these crystals confirm the results of Verweel and Roovers. Their measurements on Si-doped YIG showed n-type conductivity, however the values of the conductivity and activation energy

reported do not agree with values obtained by ourselves and other authors, probably due to the presence of a counterdope in the samples.

Measurements of the temperature dependence of both the Seebeck coefficient and the d.c. conductivity on n-type YIG have been made by ELWELL and DIXON [4] and by KSENDZOV *et al.* [14]. In fig. 1 their results are shown together with resistivity data obtained by FONTANA and EPSTEIN [8]. The resistivity of Si-doped YIG is about $10^4\ \Omega$ cm at room temperature and the activation energy is near 0.3 eV. No anomaly in the $\log \varrho$ *vs.* $1/T$ plots is observed at the Curie temperature (562 K).

The reduced Seebeck coefficient shown in fig. 1 for the Hf- as well as the Si-doped crystal in the intermediate temperature range ((250 ÷ 600) K) de-

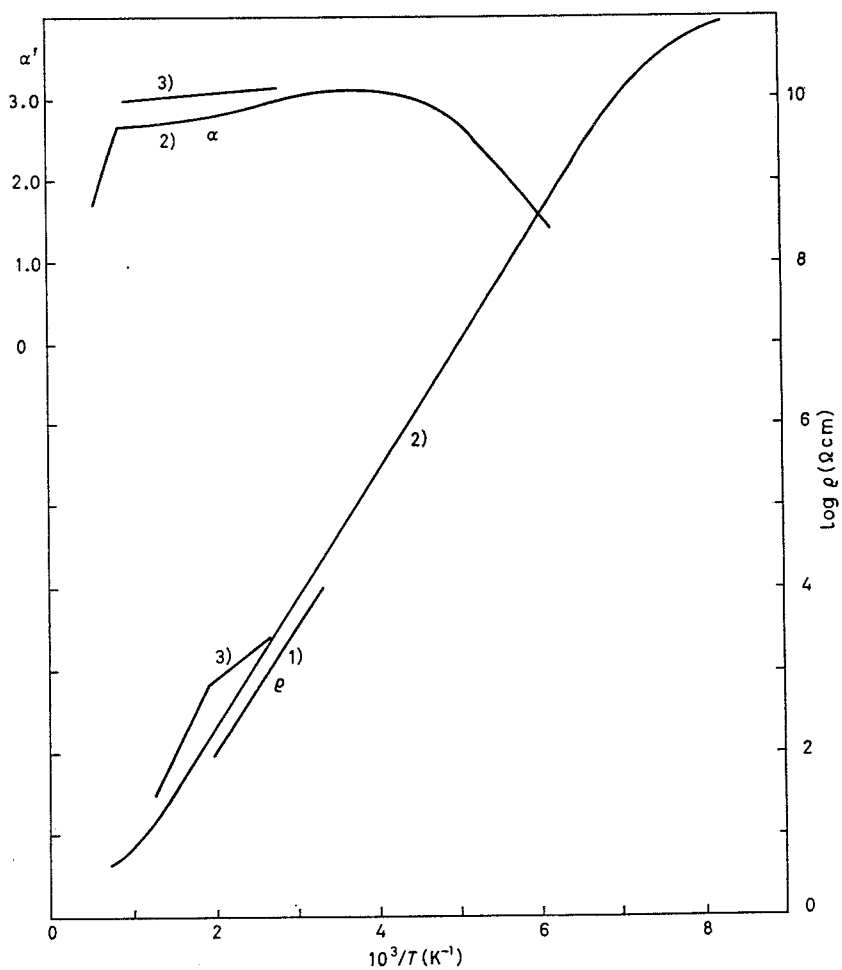

Fig. 1. – The temperature dependence of the electrical resistivity ϱ and the reduced Seebeck coefficient α' for single crystalline n-type YIG. Curve 1) Si-doped YIG (after [8]); curve 2) Si-doped YIG (after [14]); curve 3) Hf-doped YIG (after [4]).

pends only weakly on temperature. In the case of large-polaron conduction one would expect equal slopes in the plots of $\log \varrho$ and α' *vs.* $1/T$. As already concluded by ELWELL and DIXON and by KSENDZOV *et al.*, the behaviour found is more indicative of a localized hopping rather than of a band model.

Hall measurements on Si-doped YIG have been reported by BULLOCK and EPSTEIN [7]. They found that the Hall mobility has a temperature-independent value of $\mu_H \sim 0.1\ \mathrm{cm^2/Vs}$, over the range $(300 \div 1000)$ K. Figure 2 displays results obtained by KSENDZOV *et al.* [14]. The Hall mobility, which is about $0.4\ \mathrm{cm^2/Vs}$ at room temperature, decreases with increasing temperature. Such a temperature dependence of μ_H rather suggests large- than small-polaron conduction.

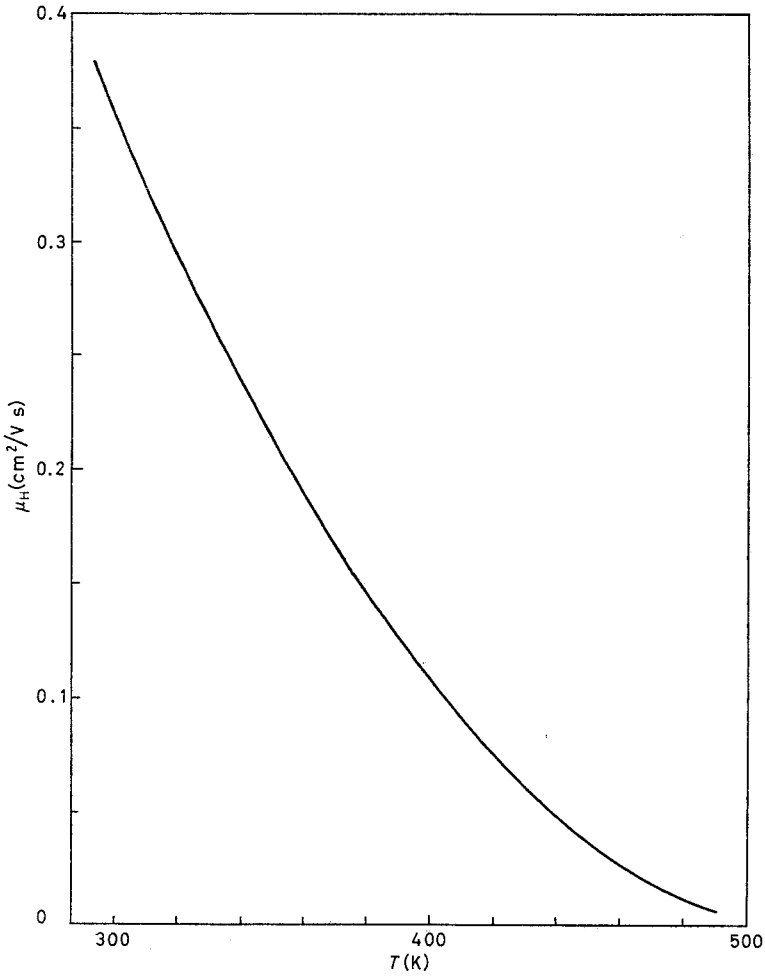

Fig. 2. – The temperature dependence of the Hall mobility for Si-doped YIG (after [14]).

On the basis of the available data it therefore seems impossible at the present time to establish the conduction mechanism in n-type YIG. Extensive measurements on a series of crystals having various concentrations of tetravalent dopants like silicon would be most useful. For p-type YIG the situation is even less clear. The Seebeck-coefficient results by VERWEEL and ROOVERS are the only ones reported. On the basis of their data solely, no conclusions on the conduction mechanism in p-type YIG can be drawn.

The reduced Seebeck coefficient shown as curve 2) in fig. 1 has a maximum at 250 K and decreases with decreasing temperature. Such behaviour has been observed in NiO and α-Fe_2O_3 too and has been ascribed to the competition of impurity conduction at low temperatures [28]. This would also explain the decrease in activation energy of ϱ at low temperatures (curve 2)). HISATAKE [19] has observed a rather discontinuous decrease in the activation energy of ϱ (from 0.65 eV above 250 K to 0.05 eV below 250 K). It should be remarked that curve 2) shows a dramatic change in slope near 1000 K; this behaviour has not been confirmed in our high-temperature measurements. Seebeck-coefficient measurements on high-ohmic samples (*i.e.* in the low-temperature region) may be influenced if the contacts are nonohmic. As long as the Seebeck results presented in fig. 2 have not been confirmed by more systematic investigations, they should be considered with some scepticism.

Thin films of YIG grown at various temperatures by liquid-phase epitaxy from a PbO-based flux have also been investigated [15]. It was found that divalent Pb was incorporated from the flux in the garnet lattice making the films p-type when grown at low temperatures. The p-type films at room temperature have a conductivity typically in the range of 10^{-6} to 10^{-7} $(\Omega\ \mathrm{cm})^{-1}$ with an activation energy of about 0.4 eV. Oxygen vacancies were found to act as donors.

Finally, a current-controlled negative resistance has been observed in single crystalline as well as polycrystalline Si-doped YIG [7, 9, 10].

3·2. *Dielectric properties.* – Information on the charge carriers bound to centres can be obtained from measurements of the a.c. conductivity and dielectric-loss measurements. CREVECOEUR [6] measured dielectric losses in the frequency range 60 Hz ÷ 1 MHz on a series of polycrystalline samples of $Y_3Fe_{5-x}Si_xO_{12}$, with $0.005 \leqslant x \leqslant 0.03$, at temperatures between 40 K and 200 K. The frequency dependence of tg δ, at 77 K, is shown in fig. 3 for three samples with different silicon concentrations. The frequency at which the losses are maximum is nearly independent of the silicon concentration and the frequency dependence can be well described by a single relaxation time as shown by the calculated Debye curve in fig. 3 (dashed curve, from eq. (13c)). The insert in fig. 3 shows that the height of the loss peak, $(\mathrm{tg}\ \delta)_{\max}$, is proportional to the silicon content and the Fe^{3+} content (see, however, the remarks on chemical analysis in the introduction). The concentration N of dipoles is therefore de-

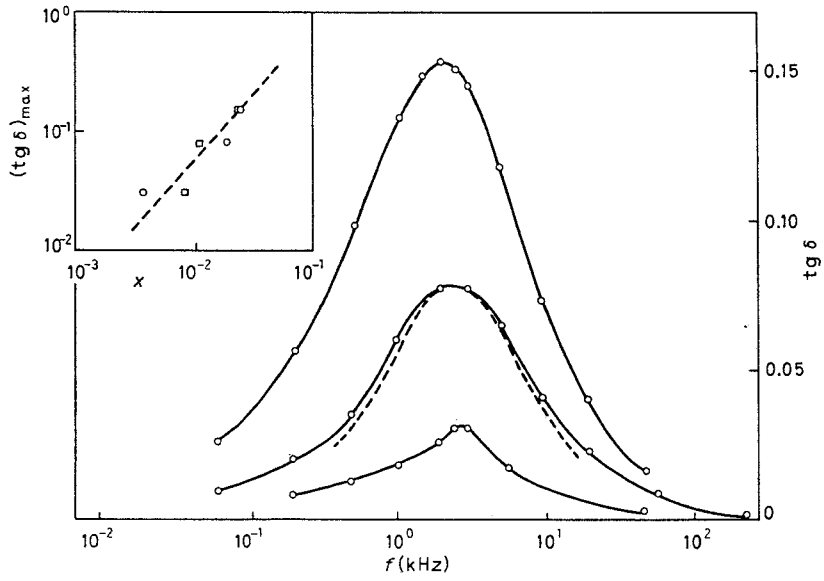

Fig. 3. – The frequency dependence of the dielectric-relaxation losses at $T = 77$ K of polycrystalline Si-doped YIG (after [6]). The dashed curve is a calculated Debye curve. Inset: The maximum height of the loss peaks in $Y_3Si_xFe_x^{2+}Fe_{5-2x}O_{12}$ at 77 K as a function of the analysed Si and Fe^{2+} concentration: o Fe^{2+}, □ Si^{4+}.

termined by the silicon concentration and from the measured value of $\varepsilon_s - \varepsilon_\infty$ the dipole moment can be calculated by using eq. (15). The resulting value of the dipole moment is $p = 1.2 \cdot 10^{-17}$ dyn$^{\frac{1}{2}}$ cm^2. The calculated value for a dipole consisting of a charge $+ e$ at a tetrahedral site (the site of the Si^{4+} atom) and $- e$ at the neighbouring octahedral site is $p = 1.7 \cdot 10^{-17}$ dyn$^{\frac{1}{2}}$ cm^2. The difference between the measured and the calculated dipole moment may be ascribed to a reduced length of the dipole due to Coulomb attraction or to the presence of a counterdope. It therefore seems reasonable to assume that the dielectric relaxation in Si-doped YIG results from the presence of dipoles formed by a Si^{4+} ion and an electron (Fe^{2+} ion) localized at one of the neighbouring octahedral sites.

From an investigation of the temperature dependence of the dielectric loss it follows that the picture of a single Si^{4+}-Fe^{2+} dipole is over-simplified. Below 77 K a broadening of the loss peak was observed [7], indicating a spread in relaxation times. We assume that this spread is due to disorder, originating from internal, locally varying electrical fields. It is interesting to note that both measurements of ferromagnetic resonance [36] and of photomagnetic effects [37] in YIG:Si lead to a similar concept of a « disorder potential ».

High-frequency conduction of a silicon-doped YIG single crystal has been investigated by FONTANA and EPSTEIN [8]. These authors measured the con-

ductivity at various frequencies up to 11 GHz in the temperature range (293 ÷ ÷ 473) K. The conductivity was found to consist of a d.c. term plus a frequency-dependent term, $\sigma(\omega)$. The latter contribution could be fitted to the form

$$\sigma(\omega) = \sigma_\infty \omega^2 \tau^2/(1 + \omega^2 \tau^2)\,, \tag{29}$$

where σ_∞ is the asymptotic value of $\sigma(\omega)$ for $\omega \to \infty$. This behaviour may be attributed to localized electrical dipoles as seen from eqs. (13*b*) and (14). With the aid of eqs. (14) and (15) the dipole moment was determined: $p = 0.8 \cdot 10^{-17}$ dyn$^{\frac{1}{2}}$ cm^2. This value is again rather low compared to the theoretical one, but this is quite probably due to the insertion of the nominal value of the silicon concentration in eq. (15), instead of an analysed concentration, or to the presence of a counterdope, *e.g.* Pb. Using eqs. (13*b*), (14) and (15) one finds $\sigma_\infty = Np^2/bkT\tau$, or $\tau = \text{const}/\sigma_\infty T$. From the observed temperature dependence of σ_∞ it is found that the relaxation time is thermally activated, $\tau = \tau_0 \exp[Q/kT]$ with $\tau_0 \approx 2 \cdot 10^{-13}$ s and $Q = 0.28$ eV. Once we know τ, the mobility of the electron bound to the Si centre can be calculated: $\mu = d^2 e/2\tau kT$. Here d is the dipole length, $d \sim 3.5$ Å. At room temperature $\tau = 7.5 \cdot 10^{-10}$ s and we find $\mu = 3 \cdot 10^{-5}$ cm^2/Vs. This is a very low value compared with the value of about 0.1 cm^2/Vs found for free electrons. We, therefore, conclude that electrons bound to silicon centres are localized on the neighbouring octahedral sites, so that electrical dipoles are formed. According to the small mobility of the bound electrons, these can be considered as small polarons.

The dielectric properties of Ca-doped *p*-type polycrystalline YIG have been measured at temperatures between 80 and 700 K at frequencies up to 36 GHz by SAMOKHVALOV *et al.* [5]. It was found that the complex dielectric constant bears a relaxation character with $\tau_0 = 3 \cdot 10^{-15}$ s and $Q = 0.4$ eV. However, τ_0 and Q were found to be somewhat frequency dependent and apparently the dielectric losses also include other types of losses than those of the Debye type. On the basis of these data a definite conclusion concerning the nature of the bound change carriers in *p*-type YIG cannot be drawn.

3·3. *Inhomogeneous conduction.* – The d.c. conductivity and the dielectric properties of *n*-type undoped polycrystalline YIG were investigated by LARSEN and METSELAAR [12, 13]. The samples were found to be macroscopically inhomogeneous exhibiting a nonohmic behaviour.

The inhomogeneity of the polycrystalline YIG samples is caused by the preparation procedure. During the sintering procedure at 1430 °C in oxygen the garnet reduces slightly, *i.e.* oxygen vacancies are formed. During cooling re-oxidation takes place. In the first stage of cooling, oxygen diffusion may be fast enough to maintain equilibrium between gas atmosphere and sample.

At lower temperatures, however, re-oxidation occurs preferentially along grain boundaries. In this way good conducting grains are separated from each other by thin high-ohmic boundary layers. This is demonstrated in fig. 4, where the frequency dependence of the conductance G and the apparent relative dielectric constant ε_r at $T = 318$ K is shown. Both G and ε_r have a frequency dependence in accordance with eq. (25). ε_s is about 200 times ε_∞, the latter having the same value as in single crystalline YIG ($\varepsilon_i = 18$). The thickness

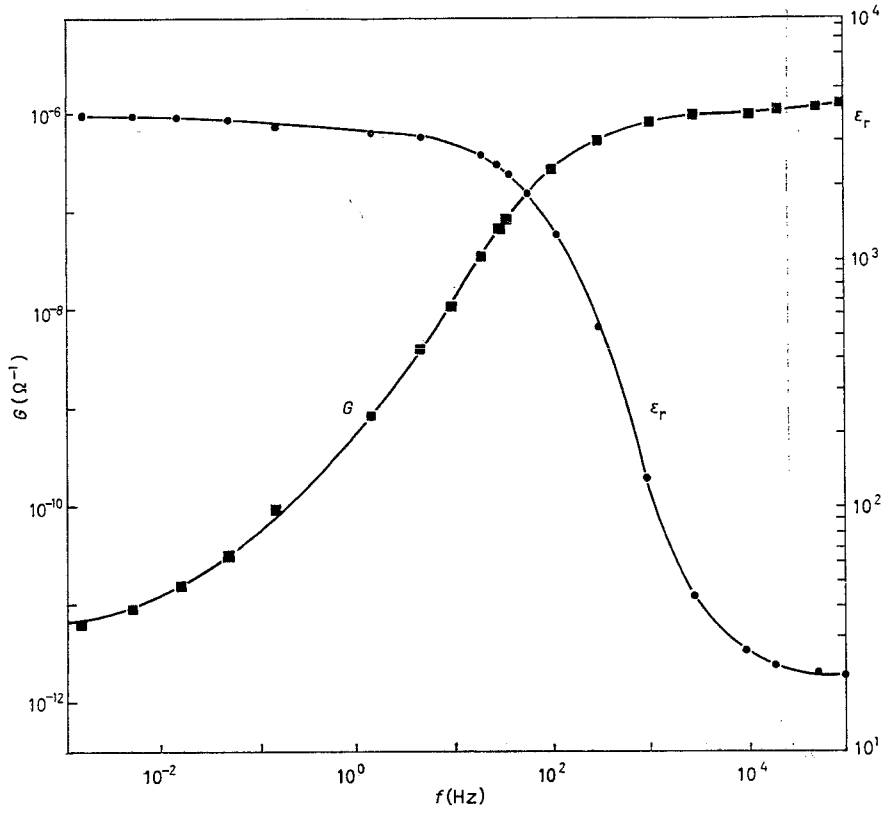

Fig. 4. – Conductance and relative dielectric constant at $T = 318$ K as a function of frequency for undoped polycrystalline YIG (after [12]).

of the high-ohmic layers can then from eq. (26*a*) be estimated to be 200 times smaller than the thickness of the grains. The static conductance is about 10^5 times smaller than the high-frequency conductance. This implies (eq. (26*b*)) that the conductivity of the grain boundaries is about $2 \cdot 10^7$ times smaller than the conductivity of the grains.

The a.c. measurements had to be made at small applied voltages (< 10 volt) in order to avoid nonohmic effects. In fig. 5 the dependence of the d.c. current on the voltage is shown for two electrode distances L. In a limited voltage

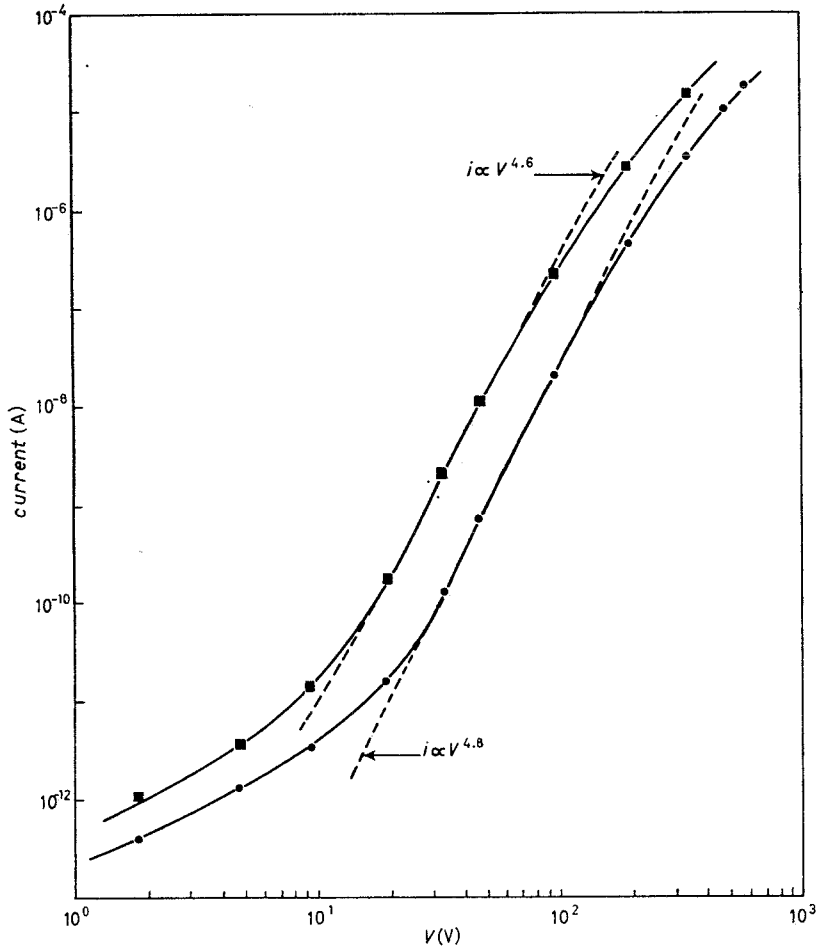

Fig. 5. – A double logarithmic plot of the d.c. i-V characteristic at $T = 295$ K for undoped polycrystalline YIG (after [12]): ▪ $L = 125\ \mu$m, • $L = 188\ \mu$m.

range above 10 V the relationship between i, V and L can be described by eq. (28) with $\gamma = 4.6 \div 4.8$ and $\beta = 7.3$. The very steep increase of current with voltage in this range is caused by injection of charge carriers, *i.e.* electrons, from the relatively good conducting grains into the high-ohmic boundaries. The injected space charge is trapped in the always present electron traps, thereby raising the quasi-Fermi level. From the temperature dependence of γ the trap distribution $\mathcal{N}_t(E)$ was found to be described by

$$\mathcal{N}_t(E) = (N_t/kT_t) \exp[(E - E_c)/kT_t], \tag{30}$$

where N_t and $T_t = \gamma T$ are constants characterizing the trap distribution.

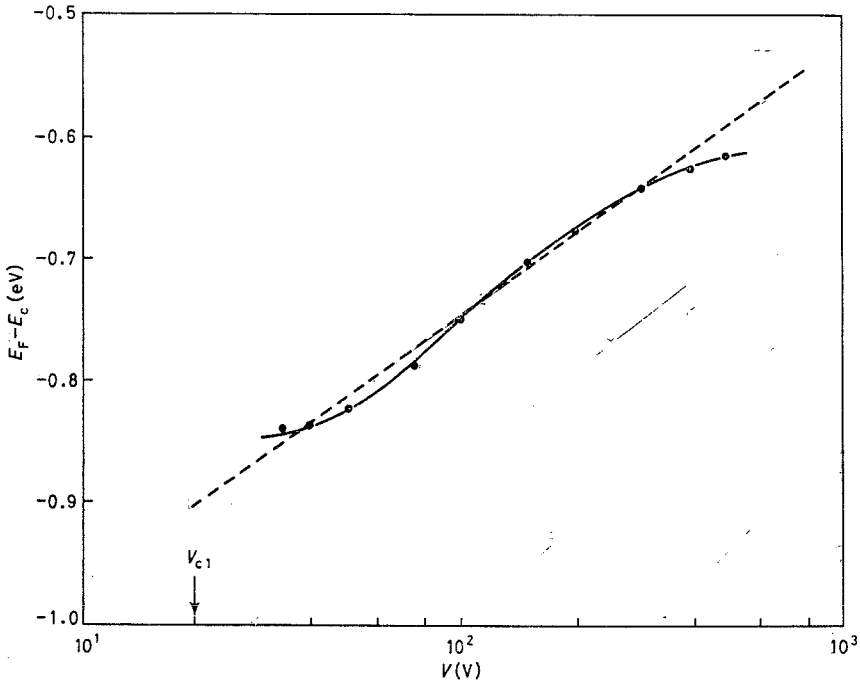

Fig. 6. – Position of the quasi-Fermi level below the conduction band at 300 K as a function of an externally applied voltage. Points: experimental data; dashed line: calculation (after [13]).

Such a quasi-continuous distribution can be thought to arise from complexes consisting of an oxygen vacancy and iron ions at various distances from the vacancy. A similar model was proposed by ENZ *et al.* to explain photomagnetic properties [37]. With this trap distribution the position of the quasi-Fermi level could be calculated. In fig. 6 a comparison between E_F directly determined from the temperature dependence of the *i vs. V* curves and E_F as calculated is shown (see ref. [13] for details). It is seen that the fit between experiments and calculations is good.

One of the important conclusions of the measurements described above is that the difference in conductivity between grain and grain boundaries is mainly due to a difference in position of the Fermi level. The explanation of these results is based on the applicability of the large-polaron band model in which the number of free charge carriers varies exponentially with temperature.

4. – High-temperature results.

In the preceding section we have seen that, in the absence of systematic measurements of d.c. conductivity, Seebeck coefficient and possibly Hall effect

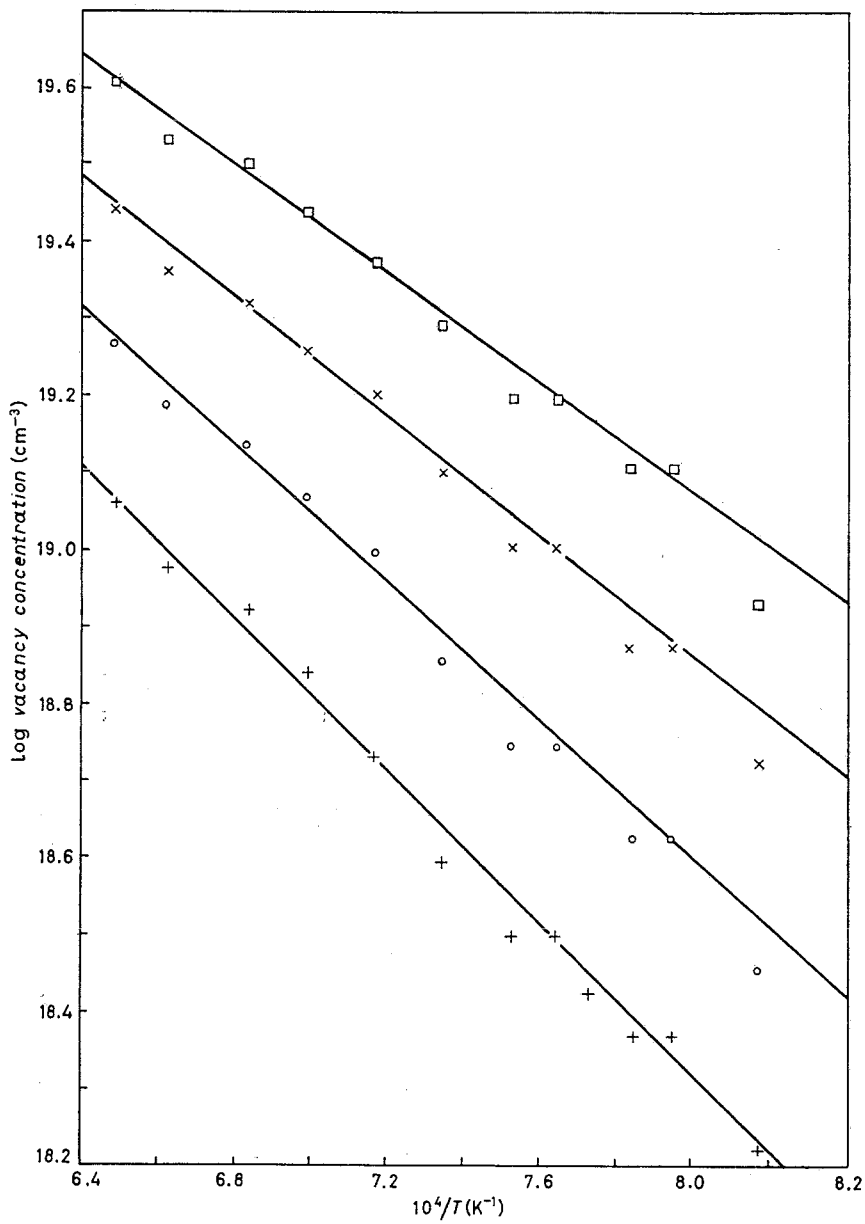

Fig. 7. – The logarithm of the oxygen vacancy concentration [V_o] in cm^{-3} as a function of the reciprocal temperature, at four different values of the partial oxygen pressure (after [18]): + 10^{-1} atm, ○ 10^{-2} atm, × 10^{-3} atm, □ 10^{-4} atm.

on series of variably doped single crystalline samples, no definite conclusions on the electrical-conduction mechanism for temperatures below 600 K can be drawn.

In the high-temperature region, (600 ÷ 1500) K, systematic measurements are greatly facilitated when use is made of the formation of native defects. After a discussion of oxygen vacancies in garnets, data on d.c. conductivity and Seebeck coefficient will be presented for the intrinsic and extrinsic range subsequently.

4·1. *Oxygen vacancies in* YIG. – Measurements of the photomagnetic effect and lattice constant measurements indicate that, at temperatures above about 1100 K, oxygen vacancies are formed in the garnet lattice [38]. From a study of the reversible weight changes of YIG, which occur by changes in the partial oxygen pressure and the temperature, the oxygen vacancy concentration can be determined. Such data obtained by thermogravimetric measurements [18] are shown in fig. 7, where the oxygen vacancy concentration is given as a function of the temperature for different partial oxygen pressures. The importance of this information stems from the fact that oxygen vacancies act as donors according to the equilibrium reaction

$$\mathrm{V_o} \rightleftarrows \mathrm{V_o^{\bullet}} + \mathrm{e'}, \tag{31a}$$

$$\mathrm{V_o^{\bullet}} \rightleftarrows \mathrm{V_o^{\bullet\bullet}} + \mathrm{e'}. \tag{31b}$$

Here we use the atomic Kröger-Vink notation, where dots indicate effective positive charges, dashes indicate effective negative charges, and subscripts indicate the atomic site of the defect. A change of the native defect concentration corresponds to a change in the total donor concentration. That means that, by varying the oxygen partial pressure in the gas surrounding the sample, the electrical properties can be changed (the temperature has to be sufficiently high to obtain equilibrium). A series of measurements at various oxygen partial pressures on *one* sample at elevated temperatures can actually be compared to a series of measurements on *differently* doped samples at low temperatures.

4·2. *Intrinsic conductivity range.* – The intrinsic conductivity range can be investigated on a sample containing divalent majority centres, *i.e.* a *p*-type sample. In fig. 8 the conductivity of a polycrystalline Mg-doped sample is shown as a function of the partial oxygen pressure at a number of temperatures. At $p_{\mathrm{O_2}} = 1$ atm the sample is *p*-type. By lowering the pressure, the concentration of oxygen vacancies, *i.e.* of donors, is increased and a decrease in the conductivity is observed. It is seen from fig. 8 that for each temperature there exists a pressure $p_{\mathrm{O_2}}^{\mathrm{min}}$ at which the conductivity reaches a minimum value

σ_{min}. For pressures lower than $p_{O_2}^{min}$ the sign of the Seebeck coefficient is negative corresponding to n-type conduction. In this pressure range the native donor concentration dominates.

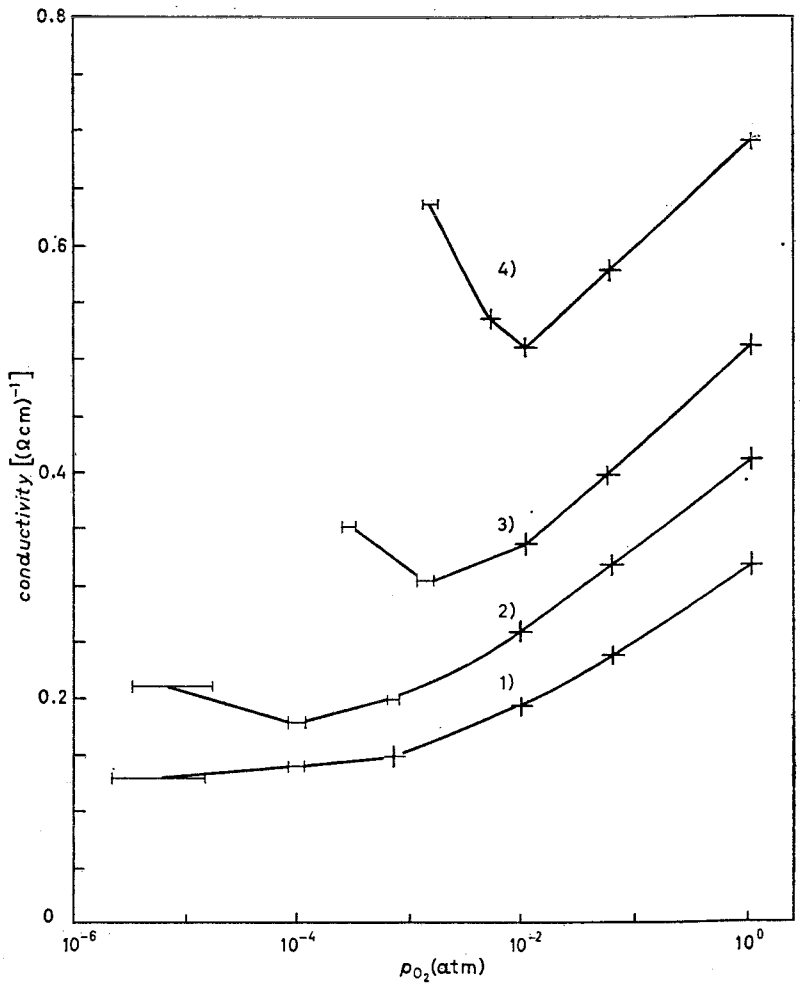

Fig. 8. – The d.c. conductivity of a polycrystalline sample $Y_3Fe_{4.98}Mg_{0.02}O_{12}$ as a function of the partial oxygen pressure at four temperatures (after [16]): 1) 1217 °C, 2) 1275 °C, 3) 1342 °C, 4) 1437 °C.

The minimum conductivity value σ_{min} is an intrinsic property which should be independent of the presence of impurities or native defects in the sample. This follows from eq. (4). In fig. 9 the values of σ_{min} measured for three different samples are shown as a function of the temperature in a $\ln \sigma_{min}$ *vs.* $1/T$ plot. The agreement between the results of the different samples is quite good.

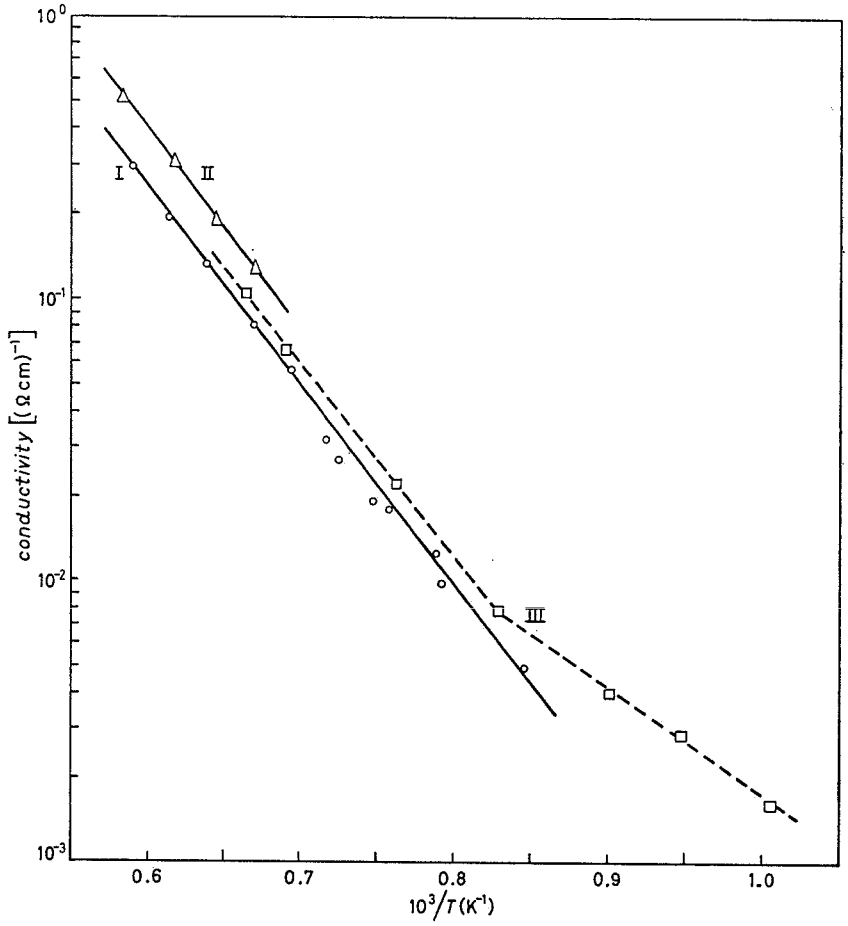

Fig. 9. – Conductivity as a function of the reciprocal temperature. For samples I and II, respectively single crystalline Ca-doped YIG and polycrystalline Mg-doped YIG, the minimum value of the conductivity is plotted. For sample III, In-doped polycrystalline YIG, σ is determined under a partial oxygen pressure of 1 atm (after [16]).

For the temperature dependence of $\sigma_{\min}$ one gets

$$\sigma_{\min} = \sigma_0 \exp[-E/kT] \tag{32}$$

with $\sigma_0 = (6.0 \pm 0.13)\cdot 10^3\ (\Omega\,\mathrm{cm})^{-1}$ and $E = 1.43$ eV. It is mostly assumed that the temperature dependence of the band gap energy E_g is described by

$$E_g = E_g^0 + \beta T\,, \tag{33}$$

where β is a constant.

If the product μN is temperature independent, it follows from eqs. (4),

(31) and (32) that $E_g^0 = 2.86$ eV. In the discussion below of the results for the extrinsic high-temperature region we shall see that this assumption for μN is indeed valid. The determination of the band gap energy can be characterized as very important. It becomes now possible to compare the energy levels of donors and acceptors relatively to each other.

The optical spectrum of YIG is so complicated that the assignment of the observed transitions is very difficult [25, 39, 40]. Our determination of E_g confirms the identification of the absorption at (2.8÷2.9) eV as a charge transfer transition.

Combined measurements of the Seebeck coefficient and of the conductivity can conveniently be plotted in a α-ln σ plot (see sect. **2**). We shall discuss such results for the intrinsic range in the next subsection.

4·3. *Extrinsic conductivity range.* – In fig. 10 the reduced Seebeck coefficient and the logarithm of the resistivity of a n-type Si-doped YIG crystal

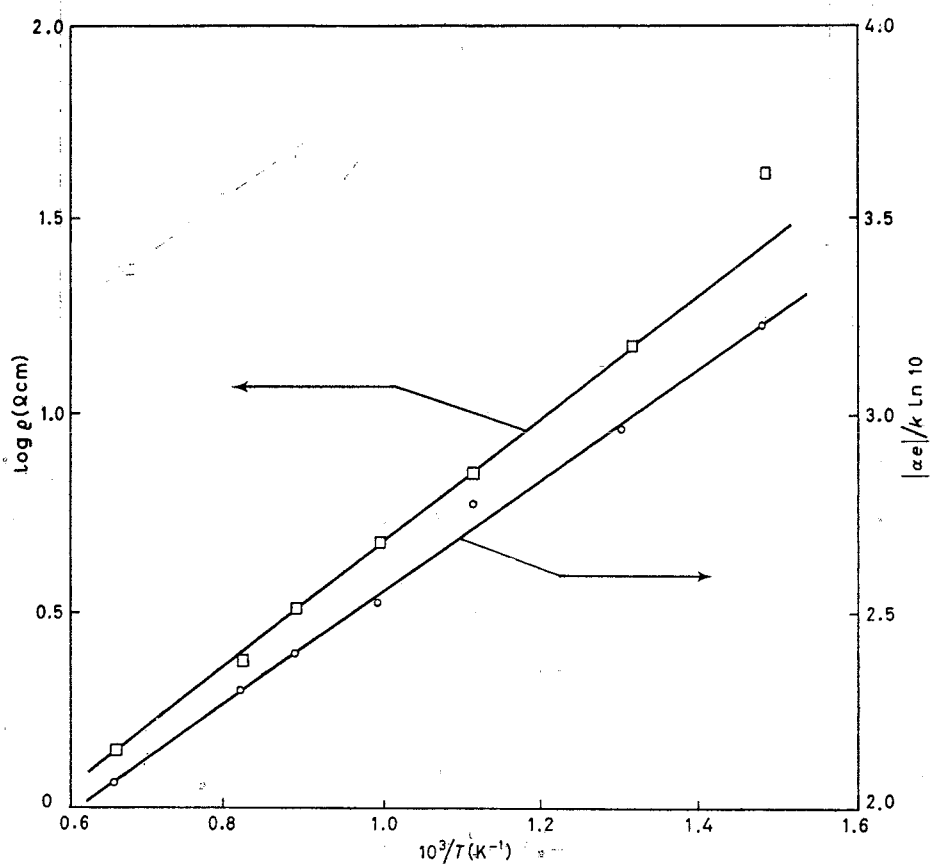

Fig. 10. – Absolute value of the reduced Seebeck coefficient and the logarithm of the resistivity of Si-doped n-type YIG (after [17]).

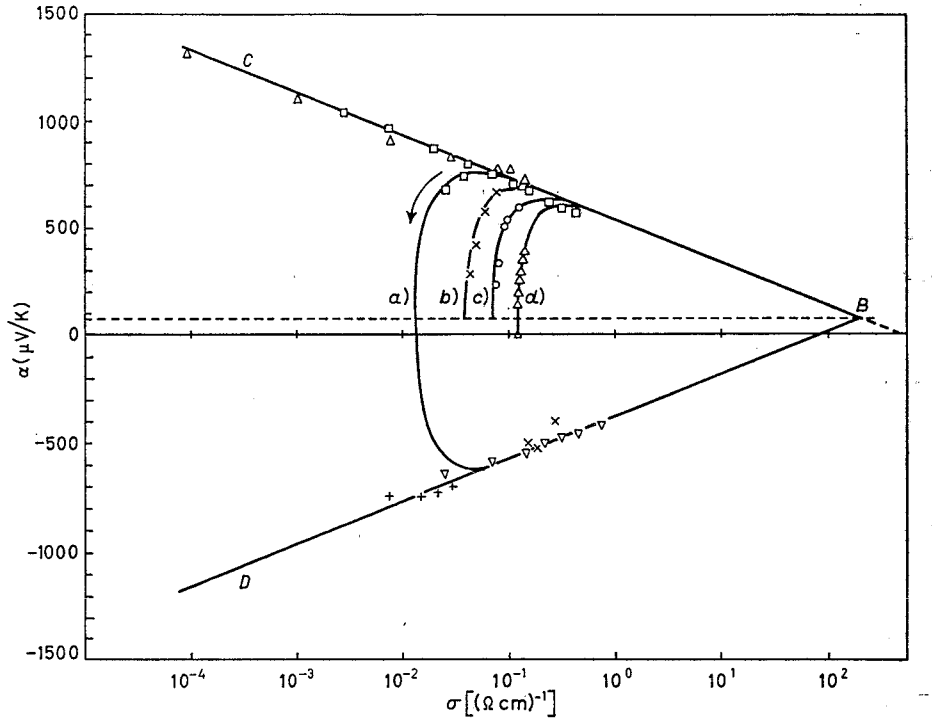

Fig. 11. – Seebeck coefficient-conductivity plot for different YIG crystals. Line *a*) $T = 1265$ K, *b*) $T = 1378$ K, *c*) $T = 1451$ K, *d*) $T = 1514$ K. Along the lines *a*)-*d*) the temperature is kept constant and the oxygen partial pressure is reduced in the direction indicated by the arrow. For points along the lines *BC* and *BD* the oxygen partial pressure is kept constant at 1 atm (after [17]).

are displayed as functions of the reciprocal temperature. The occurrence of approximately equal slopes for the α' and $\log \varrho$ curves shows that we have extrinsic conduction, and that the changes in α' and $\log \varrho$ are mainly due to the temperature dependence of n. Similar measurements were performed on another n-type YIG crystal and on two p-type YIG crystals. In all cases similar slopes for α' and $\log \varrho$ were found.

As discussed in sect. **2**, a convenient compilation of both intrinsic and extrinsic data can be given in an α-σ plot. Figure 11 contains the results obtained on a number of samples in the range of $(600 \div 1500)$ K. Points with positive α values are by definition from p-type samples, while negative α values indicate n-type samples. The intrinsic conductivity range is represented by points on the curves labelled *a*), *b*), *c*) and *d*), while points on or near the straight lines *BC* and *BD* represent the extrinsic p-type respectively n-type range. The slope of these lines is 197 μV/K, in agreement with eq. (24), *viz.* $k \ln 10 = 198$ μV/K.

Figure 11 demonstrates the internal consistency between measurements on different samples in the high-temperature range, and an analysis can be made from eqs. (7), (22)-(24), (32) and (33). For the details of the analysis, we refer the reader to ref. [16]. The main numerical results are the following:

$$\beta/k + A_+ + A_- = -5.4\,, \tag{34}$$

$$\mu_+ N_+ e^{A_+} = 3.0 \cdot 10^{21}\ (\mathrm{V\,s\,cm})^{-1}\,, \tag{35a}$$

$$\mu_- N_- e^{A_-} = 5.2 \cdot 10^{20}\ (\mathrm{V\,s\,cm})^{-1}\,. \tag{35b}$$

Additional information can be obtained from the temperature dependence of the Seebeck coefficient in the extrinsic region if eq. (21) can be applied. From the slope of the α' curve given in fig. 10 one obtains the donor ionization energy $E_d = 0.28$ eV and from the intercept at $T^{-1} = 0$ one finds

$$A_- + \ln g_- = 2.7\,. \tag{36}$$

For the p-type region a similar determination was not possible.

Now we shall briefly discuss these results in terms of the small- and the large-polaron model. We first note that the localized hopping model for YIG which was discussed in the introduction clearly is invalid in the high-temperature range. The fact that the straight lines CB and DB in Jonker's pear plot, fig. 11, represent data over a wide temperature range means that the temperature dependence of σ only can be explained by a thermal generation of the charge carriers. The possibility of a small activation energy ($\leqslant kT$) of the mobility is not excluded, however. For the small-polaron model we expect $A_- \approx 0$ and $N_- \approx 8.4 \cdot 10^{21}\ \mathrm{cm^{-3}}$. From eqs. (35$b$) and (36) one gets $\mu_- \approx 0.06\ \mathrm{cm^2/Vs}$ and $g_- \approx 15$. Since there are six equivalent cation neighbours around each Si centre, a spin multiplicity of two leads to a value $g \approx 12$ for a bound small polaron [28]. From the measurements of both CREVECOEUR [6] and FONTANA and EPSTEIN [8] it is known, however, that relaxation occurs above 120 K. This means that for the high-temperature region the g-value to be expected is much lower than 12.

For the large-polaron model $A_- = 2$ and from eq. (36) we get $g_- = 2$, which is the expected value for a free polaron in a band. The temperature independence of the product $\mu N e^A$ is in good agreement with the model. At $T = 1000$ K the density of states of the conduction band can be estimated to be given by [17] $N_- = 4.6 \cdot 10^{20}\ \mathrm{cm^{-3}}$, which gives $\mu_- = 0.15\ \mathrm{cm^2/Vs}$. This value for μ_- is rather low for the large-polaron model predicting $\mu \geqslant 0.7\ \mathrm{cm^2/Vs}$.

For p-type YIG the product $\mu N e^A$ is considerably larger than for n-type YIG and the data are highly in favour of the large-polaron model compared to the small-polaron model. Assuming both A_+ and A_- equal to 2, we get for the temperature coefficient of the band gap $\beta = -8.1 \cdot 10^4$ eV/K.

We conclude that the high-temperature data on the d.c. conductivity favour the large-polaron model.

5. – Impurities in YIG.

A few words should be added on the role of impurities in YIG. There is ample evidence that tetravalent ions like Si, Ti and Ge act as donors in the garnet lattice. Similarly divalent ions like Ca, Mg and Zn act as acceptors. In garnet single crystals grown from lead-based fluxes, lead ions are always present. Recently SCOTT and PAGE [41] suggested a self-compensation of lead in the form of Pb^{2+} and Pb^{4+}. At low concentrations Pb should be present as Pb^{2+}, while for concentrations above about 7 at% the extra Pb should be incorporated as $(Pb^{2+}Pb^{4+})$. The question whether lead is a donor or an acceptor or both, as suggested by SCOTT and PAGE, is very important for the interpretation of electrical measurements, due to the unavoidable presence of lead in single crystalline YIG. We shall therefore discuss the suggestion here.

In Scott and Page's suggestion it is assumed that both Pb^{2+} and Pb^{4+} are incorporated on the dodecahedral lattice sites. In other materials it has been observed that an impurity atom may be introduced into the host lattice with different valences if *different* sites in the lattice are available for the impurity atom. No evidence has so far been given for Scott and Page's suggestion in other materials, however.

Because the electrical conductivity is directly connected with present donors and acceptors, an investigation of the electrical properties of YIG doped with lead can be a direct test of the proposal. Such measurements have been published by LARSEN and ROBERTSON [15] and were shortly mentioned in subsect. 3·1. A plot of $\log \varrho$ as a function of the concentration difference [Pb] – [Si] shows a pronounced maximum in ϱ when the concentration difference is close to zero [24]. This maximum also coincides with a change from n-type for [Si] > [Pb] to p-type conductivity for [Pb] > [Si]. In the case [Pb] < [Si] the electroneutrality equation is approximately $[Si^{\bullet}] \simeq [Pb]_{tot}$, and E_F is close to the donor level; for [Pb] > [Si] one has $[Pb'] \simeq [Si]_{tot}$ and E_F is close to the acceptor level. At room temperature the degree of donor or acceptor ionization is low, so there will be a sharp transition when, near $[Pb] \approx [Si]$, E_F comes down from E_{donor} to $E_{acceptor}$, and the resistivity will show a sharp maximum in accordance with the experimental results. In the case of self-compensation we have an equal situation for [Pb] < [Si], but when [Pb] > [Si] we have $[Pb^{\bullet}] + [Si]_{tot} \approx [Pb']$, or $[Pb'] = \frac{1}{2}([Pb]_{tot} + [Si]_{tot})$ and $[Pb^{\bullet}] = \frac{1}{2}([Pb]_{tot} - [Si]_{tot})$. In the latter case E_F is fixed near the mean value of the lead acceptor level and the silicon donor level, *i.e.* near the centre of the band gap. This means that the resistivity should jump to a high value when [Pb] > [Si],

and it will remain there also at increasing lead concentrations. In case the acceptor ionization energy is larger than the donor ionization energy, for which there are some indications in YIG, the conductivity will always remain n-type! We conclude that there is no evidence for the occurrence of tetravalent lead ions in iron garnets. It should also be mentioned that, although trivalent lead is unusual, this paramagnetic centre has been identified in $Y_3Ga_5O_{12}$ [42]. In fact, in this compound the Pb^{3+} concentration determined from the ESR signal was of the same order of magnitude as the chemical analysed total lead concentration.

6. – Conclusions.

In the preceding sections we have surveyed the experimental results on the electrical properties of YIG for the low- and the high-temperature range. In spite of an incompleteness of experimental evidence, especially for the low-temperature range, it is possible to come to some conclusions.

Let us first consider the high-temperature region ($T > 600$ K). It is evident here that the thermal generation of the charge carriers gives the main contribution to the temperature dependence of σ for both n- and p-type YIG. This means that the localized hopping model is not applicable to YIG. The large-polaron model was found to describe the data well, however, with rather small mobilities.

In Si-doped YIG we found a donor ionization energy of 0.28 eV at high temperatures. If we note that no kink is observed at the Curie temperature in the log ϱ *vs.* T^{-1} plot and that the activation energy near room temperature is $(0.3 \div 0.35)$ eV, it seems by far most probable that the temperature dependence of σ at room temperature is still determined by a thermal generation of charge carriers. Hall measurements are in agreement with this supposition. In inhomogeneous, n-type, polycrystalline samples also the thermal generation of charge carriers was shown to be the dominant factor in σ. There are only two Seebeck-coefficient measurements in contradiction with this conclusion.

Measurements on n-type samples below room temperature indicate a substantial contribution of impurity hopping to the total conductivity.

Measurements of a.c. conductivity and dielectric loss at low temperatures show that electric-dipole losses occur due to the presence of electrons localized at sites adjacent to donor centres.

* * *

The authors wish to thank H. J. VAN DAAL and C. CREVECOEUR for discussions. Thanks are due to C. CREVECOEUR for making available the results of the dielectric-loss measurements.

REFERENCES

[1] L. G. VAN UITERT and F. W. SWANEKAMP: *Journ. Appl. Phys.*, **28**, 1513 (1957).
[2] J. VERWEEL and B. J. M. ROOVERS: *Sol. State Phys. Electr. Telecomm.*, **3**, 475 (1960).
[3] R. V. TELESNIN, A. M. EFIMOVA and R. A. YUS'KAEV: *Sov. Phys. Sol. State*, **4**, 259 (1962).
[4] D. ELWELL and A. DIXON: *Sol. State Comm.*, **6**, 585 (1968).
[5] A. A. SAMOKHVALOV, S. A. ISMAILOV and A. M. KOTEL'NIKOVA: *Sov. Phys. Sol. State*, **11**, 310 (1969).
[6] C. CREVECOEUR: unpublished results (1969).
[7] D. C. BULLOCK and D. J. EPSTEIN: *Appl. Phys. Lett.*, **17**, 199 (1970).
[8] R. E. FONTANA and D. J. EPSTEIN: *Mat. Res. Bull.*, **6**, 959 (1971).
[9] C. A. ELYARD: *Electron. Lett.*, **8**, 2 (1972).
[10] T. KAPLAN, D. C. BULLOCK, D. ADLER and D. J. EPSTEIN: *Appl. Phys. Lett.*, **20**, 439 (1972).
[11] YOUNG SOO LEE: thesis, unpublished (M.I.T., 1969).
[12] P. K. LARSEN and R. METSELAAR: *Mat. Res. Bull.*, **8**, 883 (1973).
[13] P. K. LARSEN and R. METSELAAR: *Phys. Rev. B*, **8**, 2016 (1973).
[14] YA. M. KSENDZOV, A. M. KOTEL'NIKOVA and V. V. MAKAROV: *Sov. Phys. Sol. State*, **15**, 1563 (1974).
[15] P. K. LARSEN and J. M. ROBERTSON: *Journ. Appl. Phys.*, **45**, 2867 (1974).
[16] R. METSELAAR and P. K. LARSEN: *Sol. State Comm.*, **15**, 291 (1974).
[17] P. K. LARSEN and R. METSELAAR: *Phys. Rev. B*, **14**, 2520 (1976).
[18] R. METSELAAR and M. A. H. HUYBERTS: *Journ. Sol. State Chem.*, **22**, 309 (1977).
[19] K. HISATAKE: *Trans. Japan. Inst. Met.*, **13**, 305 (1972).
[20] V. V. EREMENKO, A. P. KIRICHENKO, V. N. RUBTSOV and V. S. SMIRNOV: *Sov. Phys. Sol. State*, **14**, 1057 (1972).
[21] R. SURYANARAYANAN and R. KRISHNAN: *Phys. Stat. Sol.*, **22** (a), K 177 (1974).
[22] S. WITTEKOEK, TH. J. A. POPMA and J. M. ROBERTSON: *AIP Conference Proceedings*, No. 18 (1974), p. 944.
[23] G. H. WEMPLE, S. L. BLANK, J. A. SEMAN and W. A. BIOLSI: *Phys. Rev. B*, **9**, 2134 (1974).
[24] P. K. LARSEN and R. METSELAAR: *Journ. Sol. State Chem.*, **12**, 253 (1975).
[25] S. WITTEKOEK, TH. J. A. POPMA, J. M. ROBERTSON and P. F. BONGERS: *Phys. Rev. B*, **12**, 2777 (1975).
[26] P. K. LARSEN, R. METSELAAR and B. FEUERBACHER: *AIP Conference Proceedings*, No. 29 (1976), p. 668.
[27] K. NASSAU: *Journ. Cryst. Growth*, **2**, 215 (1968).
[28] A. J. BOSMAN and H. J. VAN DAAL: *Adv. Phys.*, **19**, 1 (1970).
[29] J. S. BLAKEMORE: *Semiconductor Statistics* (Oxford, 1962).
[30] A. YANASE: *Sol. State Comm.*, **9**, 2111 (1971).
[31] G. H. JONKER: *Phil. Res. Rep.*, **23**, 131 (1968).
[32] C. G. KOOPS: *Phys. Rev.*, **83**, 121 (1951).
[33] W. HEYWANG: *Sol. State Electr.*, **3**, 51 (1961).
[34] M. A. LAMPERT and P. MARK: *Current Injection in Solids* (New York, N. Y., 1970).
[35] H. D. JONKER: Philips Res. Lab. Eindhoven, unpublished.
[36] T. S. HARTWICK and J. SMIT: *Journ. Appl. Phys.*, **40**, 3995 (1969).

[37] U. ENZ, R. METSELAAR and P. J. RIJNIERSE: *J. Physique*, **32**, C1, 703 (1971).
[38] R. METSELAAR and M. A. H. HUYBERTS: *Journ. Phys. Chem. Sol.*, **34**, 2257 (1973).
[39] W. WETTLING, B. ANDLAUER, P. KOIDL, J. SCHNEIDER and W. TOLKSDORF: *Phys. Stat. Sol.*, **59** B, 63 (1973).
[40] G. B. SCOTT, D. E. LACKLISON, H. I. RALPH and J. L. PAGE: *Phys. Rev. B*, **12**, 2562 (1975).
[41] G. B. SCOTT and J. L. PAGE: *Journ. Appl. Phys.*, **48**, 1342 (1977).
[42] B. ANDLAUER, J. SCHNEIDER and W. TOLKSDORF: *Phys. Rev. B*, **8**, 1 (1973).